Effectiveness of fat suppression methods and influence on proton-resonance frequency shift (PRFS) MR thermometry

Anne Josset, Jonathan Vappou, Ounay Ishak, Paolo Cabras, Élodie Breton

Magnetic Resonance Imaging 118 (2025) 110340

Contents lists available at ScienceDirect

Magnetic Resonance Imaging

journal homepage: www.elsevier.com/locate/mri

Effectiveness of fat suppression methods and influence on proton-resonance frequency shift (PRFS) MR thermometry

Anne Josset [a,*], Jonathan Vappou [a], Ounay Ishak [a], Paolo Cabras [a,b], Élodie Breton [a,*]

[a] Université de Strasbourg, CNRS, INSERM, ICube, UMR7357, Strasbourg, France
[b] Image Guided Therapy, Pessac, France

ARTICLE INFO

Keywords:
Fat suppression
Fat quantification
Water-fat separation
Quantitative MRI
MR thermometry

ABSTRACT

Purpose: To evaluate the effectiveness of fat suppression techniques experimentally and illustrate their influence on the accuracy of PRFS MR-thermometry.
Methods: The residual magnitudes of the main fat peaks are measured using a water-fat decomposition algorithm in an oil phantom and in vivo in swine bone marrow, either with spectral fat saturation (FS), water excitation (WE) or fast water excitation (FWE), as implemented on 1.5 T whole-body clinical MRIs. Thermometry experiments in tissue-mimicking oil-water phantoms (10 and 30 % fat) allow determining temperature errors in PRFS MR-thermometry with no fat suppression, FS and WE, compared against reference fiber optic thermometry.
Results: WE attenuates the signal of the main methylene fat peak more than FS (2 % and 22 % amplitude attenuation in the oil phantom, respectively), while the olefinic and glycerol peaks surrounding the water peak remain unaltered with both FS and WE. Within the 37 °C to 60 °C temperature range explored, FS and WE strongly attenuate temperature errors compared to PRFS without fat suppression. The residual fat signal after FS and WE leads to errors in PRFS thermometry, that increase with the fat content and oscillate with TE and temperature. In our tests limited to a single MR provider, fat suppression with WE appears to suppress fat signal more effectively.
Conclusions: We propose a protocol to quantify the remaining fraction of each spectral fat peak after fat suppression. In PRFS thermometry, despite spectral fat suppression, the remnant fat signal leads to temperature underestimation or overestimation depending on TE, fat fraction and temperature range. Fat suppression techniques should be evaluated specifically for quantitative MRI methods such as PRFS thermometry.

1. Introduction

MR-thermometry based on Proton Resonance Frequency Shift (PRFS) [1–3] is the gold standard for the monitoring of MR-guided thermal ablations as it enables spatio-temporal temperature monitoring in real time. This technique relies on the change in the resonance frequency of the hydrogen nuclei within water molecules as temperature changes. One limit to the accuracy of PRFS thermometry comes from the presence of fat in biological tissues. Indeed, the resonance frequency of hydrogen nuclei in fat molecules is almost independent of temperature, when compared to the ones of water hydrogen [4]. The resulting temperature errors are non-linear and will vary depending on tissue fat proportion, its temperature variation, the main magnetic field B_0 and the echo time (TE) [5–7]. Hence, the signal from fat can jeopardize the outcome of thermal therapies by leading to over or under-treatment in the target area, and even to damage to surrounding healthy tissues. To mitigate this source of error, spectral fat saturation (FS) or water excitation (WE) are generally implemented in the MR-thermometry sequences used to monitor thermal therapies in fat containing tissue [8–17].

Spectral fat saturation was introduced by Haase [18] in 1985 to suppress the unwanted fat signal based on the difference in chemical shift between methylene (CH_2), the dominant fat peak, and the water peak, that difference being approximately 3.4 ppm at a temperature of 37 °C. Following a narrow band frequency-selective radiofrequency (RF) saturation pulse centered on the methylene peak frequency, spoiler gradients are employed so that no residual coherent fat signal remains during imaging. Spectral fat saturation is specifically devised to target

* Corresponding authors at: Université de Strasbourg, CNRS, INSERM, ICube, UMR7357, 1 place de l'hôpital 67091, Strasbourg, France.
E-mail addresses: a.josset@unistra.fr (A. Josset), jvappou@unistra.fr (J. Vappou), o.ishak@unistra.fr (O. Ishak), cabras@unistra.fr (P. Cabras), ebreton@unistra.fr (É. Breton).

https://doi.org/10.1016/j.mri.2025.110340
Received 14 November 2024; Received in revised form 29 January 2025; Accepted 29 January 2025
Available online 31 January 2025

the removal of the predominant methylene fat peak. With a sufficiently large bandwidth for the saturation pulse, secondary fat peaks in the vicinity of methylene are also attenuated, but further fat peaks surrounding the water peak are thought to remain unaltered. This impossibility to suppress the full fat spectra is known [19], and a correction has been designed for limiting its impact on diffusion MRI [20–22]. Furthermore, variations in the main magnetic field B_0 over time may alter the efficiency of fat saturation [23].

Alternatively, Meyer et al. [24] proposed in 1990 water selective binomial-pulse excitation to selectively target the water protons, while leaving most of the fat protons unexcited. The selectivity of the WE pulse increases with the length of their binomial chain pulse, which in turn results in longer TE. It has been shown that B_0 inhomogeneity and the contribution of multiple fat peaks alter the efficacy of water excitation in Chemical Exchange Saturation Transfer (CEST) [25].

While the value of fat suppression is no longer to be proven to enhance MRI diagnostic visualization and precision [26], the spectral effectiveness of fat suppression has, to the best of our knowledge, never been evaluated. The quantification of the remaining fat spectrum would indeed be of utmost interest in designing specific fat suppression techniques for quantitative MRI such as diffusion-weighted imaging (DWI), CEST or PRFS thermometry. In addition, the determination of the remaining fat spectrum could be used to refine correction schemes, such as those proposed for diffusion MRI that are based on theoretical values and are not system-specific.

The rationale for this work is to quantify the effectiveness of common fat suppression techniques, and to illustrate the influence of the remaining signal on the accuracy of quantitative PRFS thermometry. First, the remaining proportion of the main spectral peaks of biological fat is evaluated in an oil phantom and in vivo in swine bone marrow with FS, WE and fast WE (FWE) in clinical whole body 1.5 T MRIs. Second, the impact of the fat signal on PRFS thermometry is experimentally determined in water-fat emulsions (10 % and 30 %) during cool-down experiments for both spectral fat saturation and water excitation compared to the reference PRFS without fat suppression technique.

2. Theory

2.1. Fat spectrum and fat suppression

The typical NMR spectrum of biological fat is characterized by the presence of six main resonance peaks, each corresponding to different lipid environments within fat molecules [27–32]. While the predominant component of the fat signal comes from the methylene peak (CH_2), about 30 % originates from other peaks within the fat spectrum (Table 1).

In the context of spectral fat suppression techniques, it is notable that the two secondary fat peaks in terms of amplitude, namely the α-olefinic and methyl peaks, directly surround the methylene peak, while standing more than 2.5 ppm away from the water peak at 37 °C. Consequently, the suppression of their signal, which represents about 20 % of the total fat signal amplitude, is tightly knot to the one of the methylene peak. On the opposite, the proximity of the glycerol and olefinic peaks to the water peak strongly limits the possibility to suppress their signal spectrally. This means that about 9 % of the total fat signal is inherently neither attenuated by spectral fat suppression nor water excitation. In the field of diffusion MRI, this residual fat component is identified as a factor requiring correction in the complex signal models [20–22].

2.2. Signal model

The acquired MR complex signal, S_{TE}, from a voxel containing water and fat at a specific TE can be described as follows considering the water proton frequency drift with temperature [28,33]:

$$S_{TE} = \left(\rho_W e^{i\gamma B_0 \alpha \Delta T TE} + \rho_F \sum_{p=1}^{P} \alpha_p e^{i2\pi \Delta f_p TE}\right) e^{i2\pi\varphi TE} e^{-R_2^* TE} \quad (1)$$

Where ρ_W and ρ_F represent respectively the complex-valued intensity of water and fat components, Δf_p is the frequency of the pth fat peak relative to water at the considered baseline temperature (generally 37 °C) and α_p is its relative amplitude with $\sum_{p=1}^{P} |\alpha_p| = 1$. γ corresponds to the hydrogen gyromagnetic ratio, B_0 the main magnetic field strength, α the temperature coefficient of the water proton electron screening constant (−0.01 ppm/°C) and ΔT is the temperature change from the baseline temperature. φ is the shift caused by the B_0 field inhomogeneity and R_2* the assumed common relaxation rate for fat and water.

2.3. Fat quantification with IDEAL algorithm

The IDEAL (Iterative Decomposition of water and fat with Echo Asymmetry and Least-squares estimation) algorithm [34] stands as a robust technique for the separation and the quantification [35] of water and fat signals from complex-image data. Inspired by the Dixon method [36,37], it allows separating components with distinct chemical shifts from complex images acquired with different echo times. The IDEAL algorithm [28,38] for fat quantification relies on the signal model in Eq. (1) simplified assuming the temperature being constant:

$$s_{TE} = \left(\rho_W + \rho_F \sum_{p=1}^{P} \alpha_p e^{i2\pi \Delta f_p TE}\right) e^{i2\pi \Psi TE} \quad (2)$$

In this formulation, the complex term Ψ corresponds to a real component φ accounting for B_0 field inhomogeneity and an imaginary component addressing the R_2* decay, as follows:

$$\Psi = \varphi + i\frac{R_2^*}{2\pi} \quad (3)$$

In general, the relative amplitude and chemical shift of fat components is supposed to be known and constant between organs and individuals. It is a reasonable assumption for fat frequencies as they exhibit minimal variability across different tissue types [28]. However, a few studies [39,40] have suggested that the relative amplitudes of the fat peaks may vary among different individuals and organs. Hence, Yu et al. [28] introduced a variation of the IDEAL algorithm allowing the calibration of fat peak amplitudes α_p in order to account for their biological variability. It is worth noting that the algorithm does not directly

Table 1
Values of frequency shift relative to the water peak (ppm) and relative amplitude for each fat peak normalized by the water peak amplitude.

Peak	Name	Chemical formula	Frequency shift at 37 °C (ppm) relative to water peak	Relative amplitude		
				Human liver triglyceride [27,32]	Human breast [28]	Peanut oil [28,30,31]
1	Olefinic	–CH=CH–	0.6	0.047–0.048	0.08	0.07–0.10
2	Glycerol	–CH_2–O–CO–	- 0.4	0.039	–	0.04–0.05
3	Diacyl	–CH=CH–CH_2–CH=CH–	- 1.9	0.004–0.006	–	0.02–0.03
4	α-olefinic	–CH_2–CH=CH–CH_2–	- 2.6	0.12–0.128	0.08	0.15
5	Methylene	–$(CH_2)_n$–	- 3.4	0.693–0.70	0.85	0.62
6	Methyl	–$(CH_2)_n$–CH_3–	- 3.8	0.087–0.088	–	0.08–0.10

determine the relative amplitudes of fat peaks, but rather the signal intensity $\rho_F\alpha_p$. Since $\sum_{p=1}^{P}|\alpha_p| = 1$ by definition, it is straightforward that the fraction of each fat peak can be retrieved as:

$$|\alpha_p| = \frac{|\rho_F\alpha_p|}{\sum_{p=1}^{P}|\rho_F\alpha_p|} \quad (4)$$

Based on this work, the present study aims to determine the relative variation in magnitude of the fat spectrum in the presence of fat suppression means. Considering ρ_W and ρ_F constant between reference and fat-suppressed images, the acquired MR complex signal s_{TE}^{FSup} acquired in the presence of fat suppression methods at a specific *TE* can be described as:

$$s_{TE}^{FSup} = \left(\rho_W + \rho_F\sum_{p=1}^{P}\alpha_p^{FSup}e^{i2\pi\Delta f_p TE}\right)e^{i2\pi\Psi^{FSup}TE} \quad (5)$$

Assuming that ρ_F is constant between reference and fat-suppressed images allows direct comparison between α_p and α_p^{FSup}. Following this assumption entails that $\sum_{p=1}^{P}|\alpha_p^{FSup}| \neq 1$, while $\sum_{p=1}^{P}|\alpha_p| = 1$ by definition. This discrepancy reflects the difference in the apparent fat composition between fat-suppressed images and reference images without fat suppression.

Following this model, the effective suppression of each spectral fat peak can be quantified compared to unsuppressed fat signal. In this work, the fat spectrum is modelled considering its main five peaks; the diacyl peak is not part of this model, as its relative amplitude was shown to be negligible compared to the other main five fat peaks by spectroscopy in human triglycerides (Table 1).

2.4. PRFS thermometry

Temperature change ΔT can be evaluated from the water phase Φ using the PRFS method [1–3]:

$$\Delta T = \frac{\Phi - \Phi_0}{\alpha\gamma B_0 TE} \quad (6)$$

where Φ_0 is the reference water phase acquired at the reference temperature. In practice, the fat signal in Eq. (1) is considered neglectable with low tissue fat content and/or when employing fat suppression techniques. Hence the phase within each voxel is considered as reflecting the aqueous phase only in Eq. (6). However, any residual fat component will lead to erroneous measurements. Following the assumption of pure water signal, the sensitivity of PRFS thermometry is theoretically maximal when TE equals the tissue's T_2* [41]. In practice, the TE of fast gradient echo sequences is typically chosen between 10 and 20 ms for monitoring thermal ablations [8,10–12,42,43].

3. Materials and methods

First, the effectiveness of FS, WE and FWE was quantified experimentally both in peanut oil and in vivo on porcine bone marrow. Second, the temperature errors in PRFS-thermometry due to the signal of fat without and with FS or WE were evaluated in phantoms depending on both TE and phantom fat fraction. Data processing was performed within the Matlab software (Mathworks Inc., MATLAB R2023a).

3.1. MRI acquisitions

Experiments were conducted in two whole body 1.5 T clinical MRIs (MAGNETOM Sola (phantoms) and Aera (in vivo), Siemens Healthineers, Erlangen, Germany). For all experiments, the phantom was positioned at the MRI isocenter at the center of the head coil 20 elements. The scanner central frequency was manually set to +210 Hz relative to the methylene fat peak, corresponding to the chemical shift between methylene and water at temperature 37 °C and 1.5 T, in order to standardize the spectral fat suppression effectiveness, regardless of phantom temperature. For in vivo experiments, the anesthetized swine was positioned laterally, and the thigh was imaged with the 18 elements body matrix coil combined with the spine coil. In all experiments, the shim box was manually reduced to fit the region of interest.

Images were collected using a 2D multi-echo spoiled gradient-echo (SPGR) sequence with several images acquired as an echo planar imaging (EPI) readout. Relevant parameters for the phantom acquisition were: TR 300 ms, 12 TE with monopolar EPI readouts, initial TE 4.21 ms, ΔTE 1.74 ms, FOV 192 mm × 156 mm, slice thickness 6 mm, matrix 96 × 78, readout bandwidth 1488 Hz.px^{-1}, flip angle 80°, GRAPPA factor 2, acquisition time 14 s. In vivo acquisitions in the swine leg used the same parameters except for the following: FOV 280 mm × 227 mm and flip angle 60°. With those parameters, the chemical shift of the fat signal was approximately 0.1 pixel and is neglected.

3.2. Quantification of the effect of fat suppression

The remaining fat signal was evaluated for the FS and two WE options available on our clinical MRI scanners. The "fat saturation" option features a Gaussian pulse with a 110° flip angle (bandwidth 197 Hz) followed by gradient spoiling [44]. The "water excitation" option consists in a monopolar 1–2–1 binomial pulse train [45], whereas the "fast water excitation" option relies on a shorter monopolar 1–1 binomial pulse train.

Peanut oil was chosen to mimic human fat due to the similarity reported between its nuclear magnetic resonance spectrum and the one of human fat triglycerides [28] (Table 1). The peanut oil plastic container was placed within a sugar syrup-filled larger container. Sugar syrup, a widely available water-based viscous fluid, was selected to allow for the central frequency auto-calibration of the scanner. The multiecho 2D SPGR sequence was applied with FS, WE, FWE and without any suppression technique.

Assuming that the water fraction within pure peanut oil can be neglected leads to the simplification of Eqs. (2) and (5) with only the main 5 fat peaks and no water component in the signal model of the IDEAL algorithm. In the bone marrow, this simplification was not done.

Average value and standard deviation of fat peak magnitudes were calculated within an 11 × 9-pixel Region Of Interest (ROI) selected in the middle of the peanut oil phantom, and an 4 × 4-pixel ROI in the thigh bone marrow (Fig. 1). The relative maximal fat magnitude was evaluated as $\sum_{p=1}^{P}|\alpha_p^{FSup}|$; it corresponds to the theoretical relative fat magnitude when all spectral fat peaks are in phase (TE = 0 ms).

3.3. Temperature errors without and with fat suppressed PRFS

Oil-water phantoms of 50 mL were elaborated in cylindrical containers (3 cm in diameter) according to the method of Bush et al. [46] by emulsifying agarose, water and peanut oil. Phantoms were designed to simulate organ tissues such as the liver, breast, or muscles, with targeted fat fraction of 10 % and 30 %. T_2* values obtained by the IDEAL algorithm are provided in Supplementary material (Table S1). For these two fat contents, the temperature error was determined for MR-PRFS without fat-suppression, as well as PRFS prepared with FS, and with WE. Each experiment was repeated 3 times, with different tubes.

In each experiment, a single oil-water tube was uniformly heated to 62 °C within a water bath for about 30 min. This heated tube was placed within sugar syrup in the center of three pure agar tubes used for B_0 drift monitoring, interleaved with three peanut oil-filled tubes (Fig. 2). The absolute reference temperature was logged every second with four fiber optic temperature probes (Rugged Monitoring, Québec, Canada) inserted respectively within the heated tube and the three B_0 drift monitoring agar tubes. The temperature was monitored in the heated tube with both

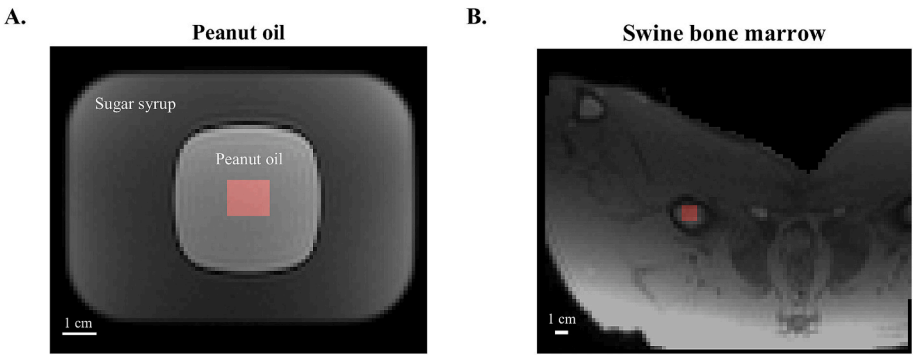

Fig. 1. Magnitude images depicting the experimental set-up for the quantification of the effect of fat suppression in the peanut oil phantom (A) and in vivo in swine bone marrow (B). Red areas represent the ROI selected to measure relative fat peaks magnitude. (For interpretation of the references to colour in this figure legend, the reader is referred to the web version of this article.)

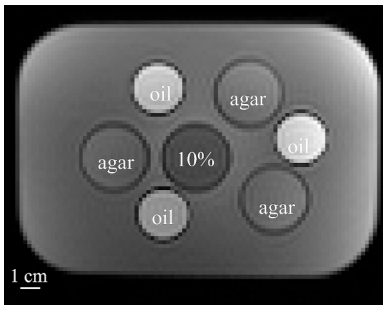

Fig. 2. Magnitude image depicting the experiment: the emulsion tube is surrounded by 3 agar tubes to correct for B_0 drift and 3 vials of pure peanut-oil.

MR PRFS and fiber optic probes during its cooling down to 37 °C (as measured with the fiber optic thermometer), chosen as the reference temperature.

The multiecho 2D SPGR sequence was parameterized with a flip angle of 60°. The temporal resolution was of 14 s for each set of 12 gradient echo images with respective TE: 4.21 - 5.95 - 7.69 - 10.3 - 12.04 - 13.8 - 15.54 - 17.28 - 19.02 - 20.76 - 22.5 - 24.24 ms. The temporal resolution was adapted for the kinetics of our cooling down experiment (typically 30 min) while ensuring sufficient signal-to-noise ratio (SNR). Phase images were B_0-drift corrected by averaging the phase in the 3 agar tubes, individually corrected for the mild (<2 °C) temperature change due to thermal diffusion from the central warm emulsion. This temperature change was measured by the fiber optic probe within each agar tube, and the corresponding phase-change was subtracted to the phase determined at the center of the agar tube. Because the PRFS method measures temperature variation, the phase time stack can be reversed to mimic the process of heating. Temperature errors were calculated for each TE within a 3 × 3-pixel square ROI drawn around the optical probe location. The temperature error was defined as the difference between the temperature variation determined using PRFS and the reference measurement from the fiber optic thermometer.

4. Results

4.1. Quantification of the effect of fat suppression

Normalized magnitude found for the 5 main fat peaks considered in peanut oil and in swine bone marrow are shown Fig. 3 and detailed in Table 2 without fat suppression acquisition, FS, WE and FWE. The magnitude of fat peaks determined without fat suppression methods are in accordance with the values given in the literature for peanut oil

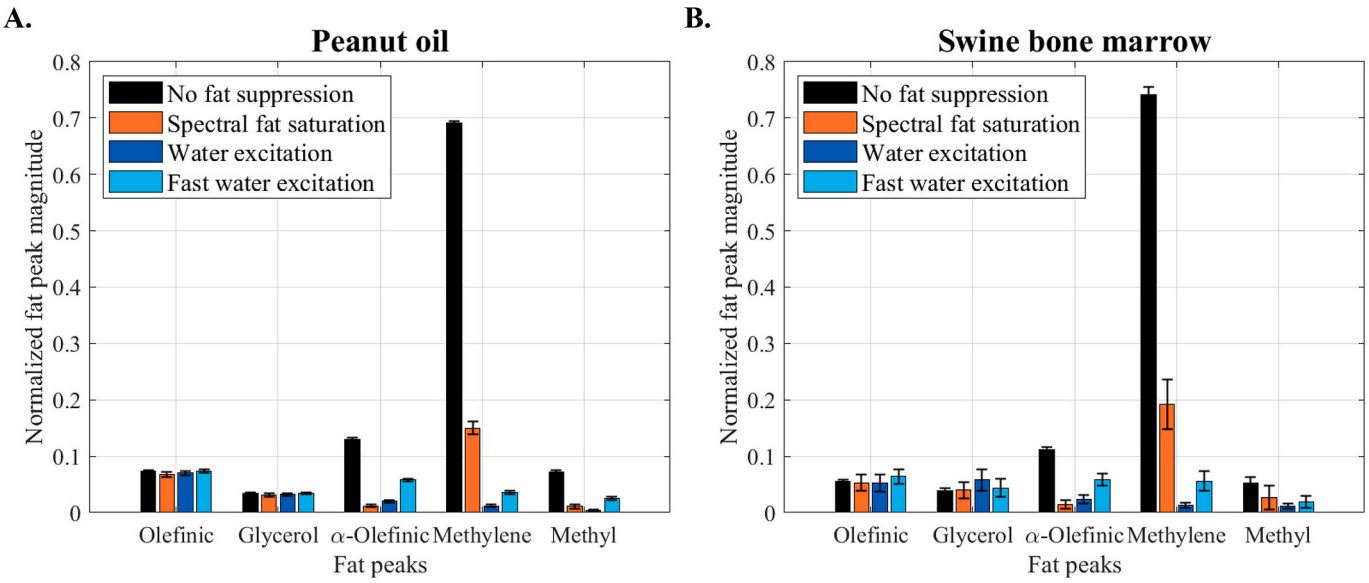

Fig. 3. Normalized magnitude $|\alpha_p|$ and $|\alpha_p^{FSup}|$ of the main 5 fat peaks in peanut oil (A) and in swine bone marrow (B) without fat suppression method, with FS, WE and FWE averaged in the ROI. Error bars represent the standard deviation over the ROI.

Table 2
Normalized fat peak magnitudes determined in peanut oil and in vivo in the bone marrow of a swine without fat suppression, with FS, with WE and with FWE. For improved readability all magnitude values are given with a factor 10^{-2}.

Fat peak		Olefinic	Glycerol	α-Olefinic	Methylene	Methyl
	Acquisition	Fat peak magnitudes [10^{-2}]				
Peanut oil	No fat suppression	7.3 ± 0.1	3.4 ± 0.1	13 ± 0.2	69.2 ± 0.3	7.2 ± 0.4
	FS	6.7 ± 0.5	3.1 ± 0.3	1.2 ± 0.2	15 ± 1.1	1.1 ± 0.4
	WE	7.0 ± 0.4	3.2 ± 0.3	2 ± 0.2	1.2 ± 0.2	0.4 ± 0.2
	FWE	7.4 ± 0.3	3.4 ± 0.2	5.8 ± 0.2	3.6 ± 0.3	2.5 ± 0.3
Swine bone marrow in vivo	No fat suppression	5.5 ± 0.4	3.8 ± 0.6	11.2 ± 0.5	74.2 ± 1.3	5.3 ± 1.1
	FS	5.3 ± 1.4	4.0 ± 1.4	1.4 ± 0.8	19.2 ± 4.5	2.7 ± 2.1
	WE	5.3 ± 1.5	5.8 ± 1.9	2.4 ± 0.7	1.3 ± 0.5	1.1 ± 0.5
	FWE	6.4 ± 1.3	4.4 ± 1.7	5.9 ± 1.1	5.6 ± 1.7	1.9 ± 1.0

[28–31].

As expected, FS, WE and FWE show no significant impact on neither olefinic nor glycerol peaks: more than 91 % persist despite fat suppression methods in the phantom, and 96 % in bone marrow. Also as anticipated, all three tested spectral fat suppression techniques significantly diminish the magnitude of methyl (15 %, 5 % and 35 % remaining for FS, WE, and FWE, respectively) and α-olefinic peaks (9 %, 15 % and 45 % remaining for FS, WE, and FWE, respectively) in the oil phantom. Logically, WE outperforms FWE due to its longer binomial pulse train. The main distinction between spectral fat saturation and water excitation as implemented on our clinical MRIs lies in their influence on the prominent fat peak, methylene. After FS, 22 % of the methylene peak persists in the peanut oil phantom, whereas only 2 % remains after WE and 5 % with FWE. When considering the fat spectrum as a whole, the relative maximal fat magnitude represents 27 %, 14 % and 23 % of the reference value with FS, WE and FWE, respectively, in the peanut oil phantom. Similar trends are found in vivo in the swine bone marrow, but with higher standard deviation because more parameters are fitted compared to pure oil.

4.2. Temperature errors in fat suppressed PRFS

A total of 18 experiments (3 repetitions for 3 suppression methods and 2 oil-water emulsions) were led, with 12 TE datasets for each experiment. Fig. 4 and Fig. 5 illustrate the variation in temperature error with TE and temperature, using emulsions with 10 % and 30 % fat fractions, respectively. Only the data for 6 TE values comprised between 10 and 20 ms, are presented, as they correspond to the typical range used for PRFS during thermal ablations. Additional TE data are available in Supplementary material Fig. S1 and S2. Fig. 6 represents the mean

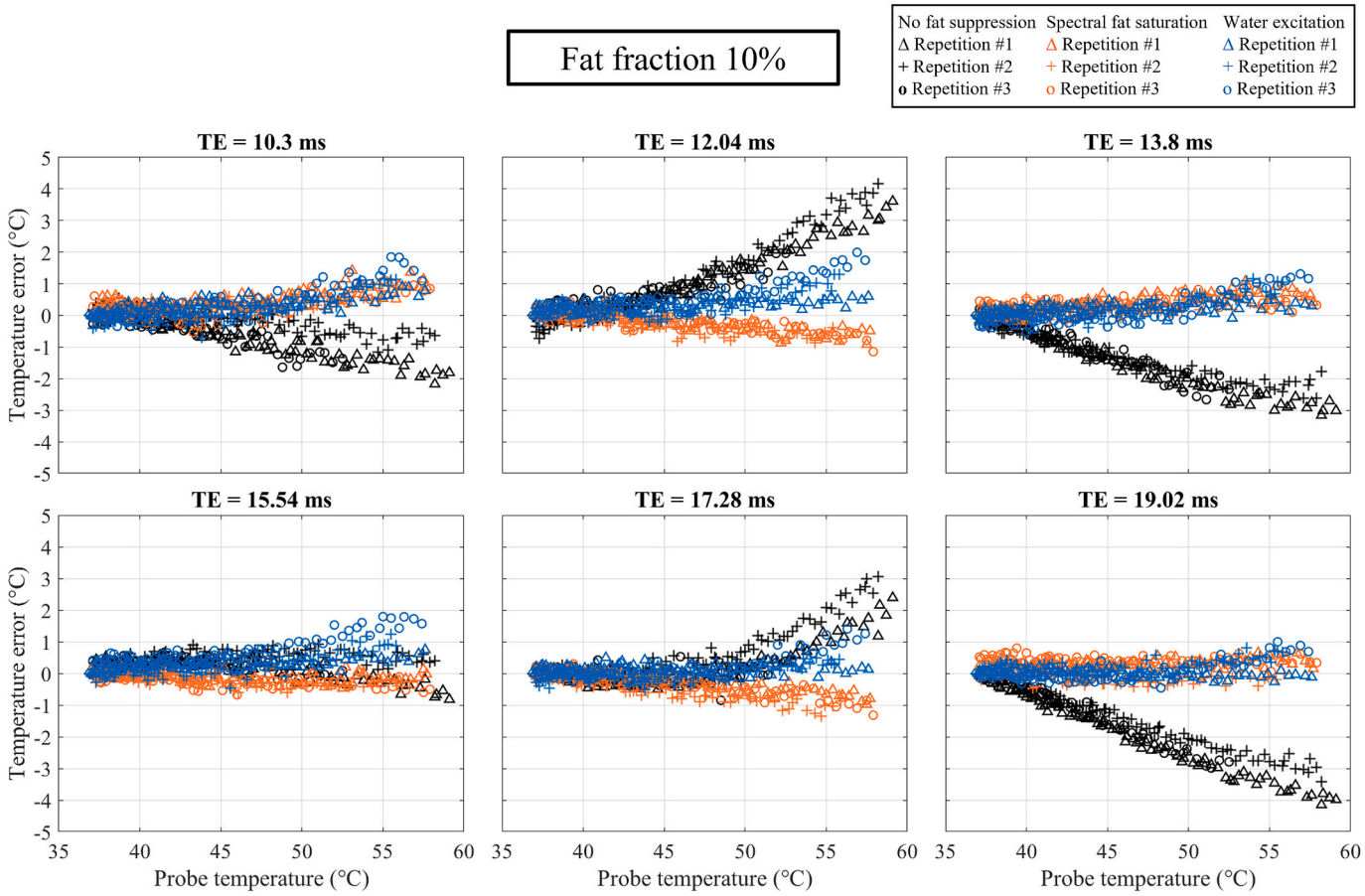

Fig. 4. Temperature errors depending on spectral fat suppression in the peanut oil-water phantoms with fat fraction 10 % during the thermometry experiments drawn for selected TEs. For each TE, temperature errors are evaluated by comparing PRFS thermometry temperature elevation measurements with temperature elevation measured by the optical probes in an ROI drawn around the position of the optical probe.

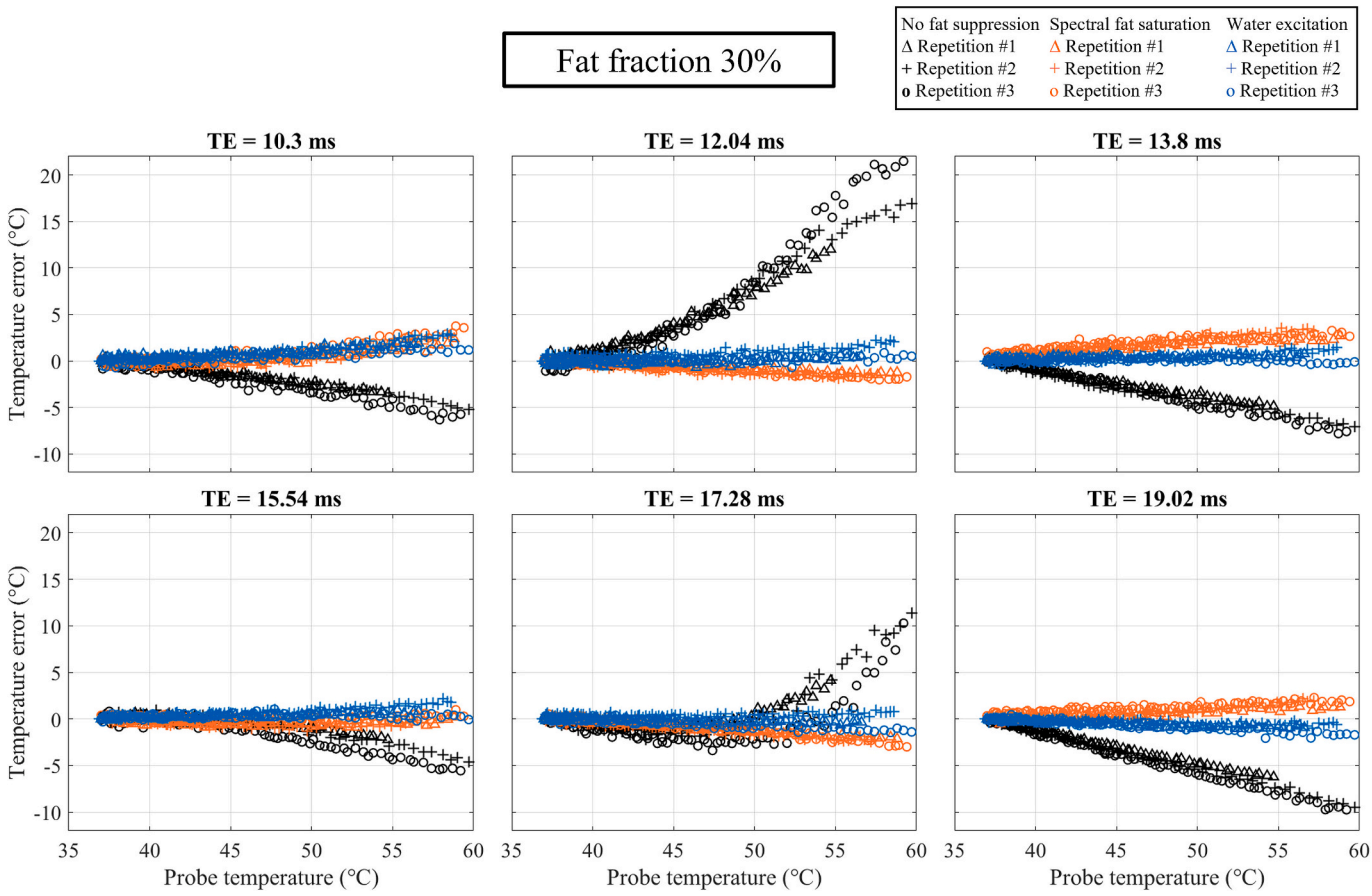

Fig. 5. Temperature errors depending on spectral fat suppression in the peanut oil-water phantoms with fat fraction 30 % during the thermometry experiments drawn for selected TEs. For each TE, temperature errors are evaluated by comparing PRFS thermometry temperature elevation measurements with temperature elevation measured by the optical probes in an ROI drawn around the position of the optical probe.

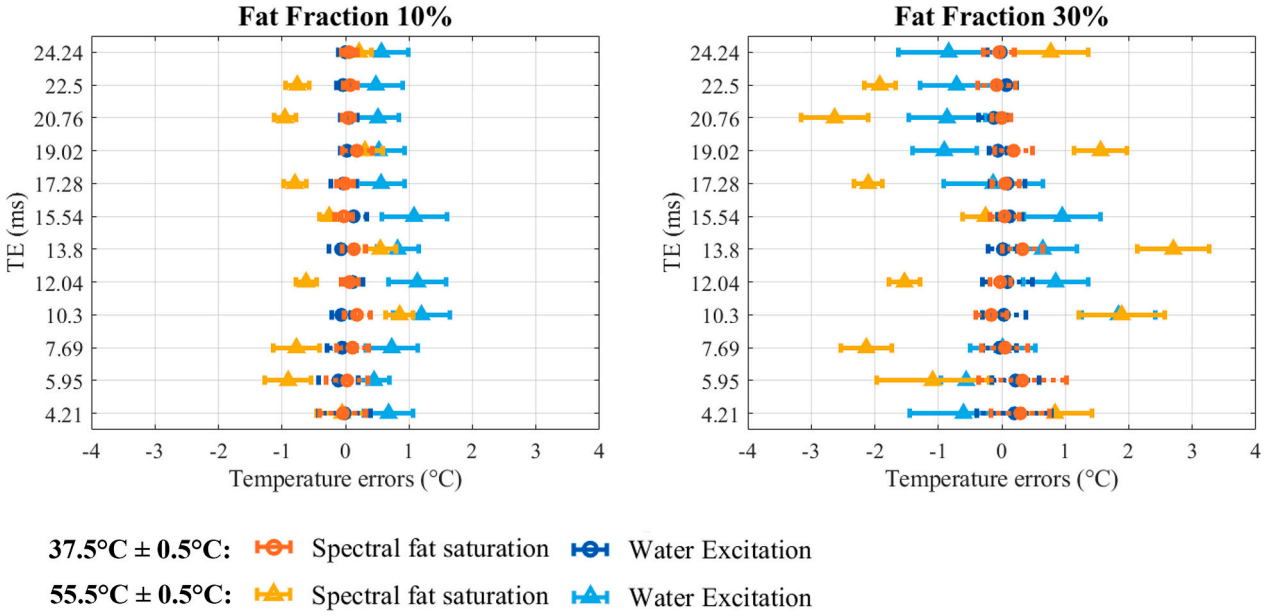

Fig. 6. Mean temperature errors and standard deviations at 37.5 °C ± 0.5 °C (circles) and 55.5 °C ± 0.5 °C (triangles) across 3 repetitions plotted against TE with FS (orange) and WE (blue) for the 10 % (left) and 30 % (right) fat emulsions. (For interpretation of the references to colour in this figure legend, the reader is referred to the web version of this article.)

temperature errors and standard deviations calculated across 3 repetitions for each of the 12 TEs and the 2 fat fractions (10 % and 30 %) at temperatures 37.5 °C ± 0.5 °C and 55.5 °C ± 0.5 °C (temperature range of 1 °C) for FS and WE. The standard deviations around 37.5 °C are all inferior to 0.7 °C (inferior to 0.4 °C for TE > 10 ms) for the two concentrations, in accordance with previously published PRFS precision [47,48].

As expected, temperature errors increase with temperature and fat fraction, and oscillate with TE (Fig. 6). For instance, PRFS with TE = 15.54 ms appears little sensitive to the presence of fat in the phantoms. Without any fat suppression method, the temperature elevation is strongly overestimated with TE = 12.04 ms, while strongly underestimated with TE = 13.8 ms and TE = 19.02 ms. For both fat concentrations at a TE of 17.28 ms, temperature errors without fat suppression remain relatively low until reaching 50 °C, after which they increase steadily.

Both FS and WE strongly limit the negative influence of the fat signal on the accuracy of PRFS with 10 % and 30 % fat fraction. Over the entire cool-down experiments (approximately 23 °C temperature range) with the 10 % fat fraction emulsion and our set of TEs between 10 and 20 ms, temperature deviations between fat suppression methods and the temperature probe vary between −1.3 °C and 2.0 °C, contrasting with the wider range of −4.1 °C to 4.2 °C observed without fat suppression. Likewise, for the 30 % fat fraction emulsion, temperature errors without fat suppression span from −9.7 °C to 21.5 °C, while employing fat suppression narrows this range to −3.0 °C to 3.7 °C. WE appears to attenuate the fat signal more effectively than FS, with less dependence on the TE (Fig. 6).

Temperature error curves are comparable between the repeated experiments which indicates a good reproducibility of the experimental protocol. The maximum temperature varies slightly across the different experiments as it depends on the delay between the heated tube being removed from the heating water bath and the effective start of the MRI acquisition.

5. Discussion

In this paper, we propose a protocol to quantify the individual remaining proportion of each fat peak after spectral fat saturation and water excitation. The influence of the remaining fat signal on the accuracy of quantitative PRFS MR-thermometry is evaluated experimentally for two different fat contents and 12 TEs between 37 and 60 °C.

Fat suppression techniques, designed for diagnostic MRI, focus on the suppression of the main fat peak, methylene. The fat spectrum, however, consists of multiple peaks that are not equivalently attenuated by spectral fat suppression. Our experimental evaluation of the magnitudes of the main five spectral peaks confirms that while the methyl and α-olefinic peaks in the direct vicinity of methylene are also strongly attenuated, those adjacent to the water peak (olefinic and glycerol) are left nearly unaffected by spectral fat suppression methods. We found WE more effective in mitigating the magnitude of the methylene peak than FS, both used as implemented by the MRI manufacturer in our clinical 1.5 T MRIs. As expected, WE was more effective in suppressing the signal of fat than FWE that relies on the shorter 1–1 binomial pulse train.

The accuracy of the quantification of the remaining fat spectrum depends on the choice of the TEs, as already studied with the IDEAL algorithm [49]. It should be noted that the proposed fat suppression quantification protocol can be applied for any fat suppression method as long as the TE can be varied. Fat suppression with inversion recuperation was not evaluated in this work as this technique is not relevant in the context of real time PRFS thermometry. Although its lower sensitivity to B_0 and B_1 inhomogeneities than spectral fat suppression might be an advantage, inversion recuperation increases the acquisition time and specific absorption rate (SAR), and may reduce the SNR of the images [50].

The error due to the presence of fat signal in PFRS thermometry was quantified experimentally in tissue-mimicking oil-water emulsions in the absence of fat suppression, with spectral fat saturation and with water excitation. Our results without fat suppression corroborate the known influence of fat fraction, temperature and TE on the temperature error [5]. In this work, we have quantified the effect of these parameters on temperature error while using fat suppression methods. Although temperature errors are considerably attenuated by both spectral fat saturation and water excitation compared to acquisitions without fat suppression, they reached up to 2 °C and 3.7 °C (absolute values) in our experiments, respectively with the 10 % and 30 % fat phantoms, over a temperature range between 37 °C and 60 °C. The errors obtained with 10 % fat after fat suppression methods are similar to the generally accepted PRFS precision [47,48], attesting an efficient suppression in the temperature range explored. In our experiments with WE and FS used as implemented by a single vendor at 1.5 T, the temperature error observed with WE is lower and less dependent on the sequence TE than the one observed with FS.

Initially, FS was designed using a 90°-saturation pulse to remove the signal of the methylene peak and the directly surrounding peaks. The glycerol and olefinic fat peaks close to the water peak are hence logically left unattenuated. Alternative methods were proposed to tackle that limitation by compensating the signal of those glycerol and olefinic fat peaks with an equivalent voluntarily left-out methylene signal [44,51,52]. A flip angle different from 90° is employed to retain a given amount of magnetization of the main fat peaks that would null the peaks close to water, when their transversal magnetizations are in-phase or out-of-phase [52,53]. The FS pulse tested in our experiments on clinical 1.5 T MRI systems appears to follow that concept with a flip angle of 110°. It is important to note that following that approach, the effectiveness of spectral fat saturation is contingent on the choice of specific TEs, as observed in our experiments. Our study examined temperature errors within the limited range of 37 °C up to 60 °C, because higher temperatures damaged the oil-water tissue mimicking agar phantoms. The minimal temperature of 37 °C was chosen to mimic clinical thermal ablations, since the reference temperature influences the sensitivity of PRFS to the fat signal. During thermal ablation procedures, higher temperatures may be encountered, which may result in larger temperature errors.

Despite the presence of fat being known to cause temperature errors in PRFS MR-thermometry, spectral fat suppression in not systematically used in clinical practice [42,43,54–56]. Some clinical studies [57,58] applied a binary mask to use different thermometry methods in areas abundant in water and those rich in fat. Nevertheless, the selection of the threshold value is based on empirical choices; typically, a water content of at least 75 %–80 % is considered to yield negligible errors. In our experiments without fat suppression, a fat percentage as low as 10 % in the phantom results in maximal absolute error of 4.2 °C, within our set of TEs between 10 and 20 ms and maximal absolute temperature of 60 °C. This maximal temperature error without fat suppression reaches as much as 21.5 °C in the 30 % fat tissue-mimicking phantoms. Therefore, caution should be taken when choosing a fat-ratio threshold for MR-thermometry without fat suppression.

To address the limitations due to the presence of fat in PRFS thermometry, it has been proposed to combine it with other MR-thermometry techniques, such as relaxation time thermometry [57,59–61]. However, these techniques usually rely on a tissue dependent calibration process [62,63] to correlate temperature with relaxation times. It has also been demonstrated that this calibration step is not necessary with relaxation time thermometry of specific fat components, which would ask for fat-water separation [64].

Spectral fat suppression techniques vary in terms of pulse shape, flip angle, duration, and timing in the chronogram, among the MRI-manufacturers, which may impact the effectiveness of fat suppression [44,53]. Tailored for diagnostic imaging, these approaches might not be the most suitable for quantitative MRI, such as PRFS thermometry, diffusion and CEST. The quantification of the effective attenuation of the

spectral components of fat could support the design of specific spectral fat suppression schemes tailored to the needs of quantitative MRI.

6. Conclusion

We propose to quantify the fat peak magnitudes for assessing the efficiency of fat suppression techniques. The experimental evaluation highlighted the intrinsic differences between the tested FS, WE and FWE methods, in terms of effective attenuation of each spectral fat peak. In the context of MR-guided thermal therapies, the remnant fat signal despite FS or WE was shown to cause absolute temperature errors in PRFS thermometry of several degrees in tissue-mimicking phantoms at 1.5 T. Users of quantitative MRI techniques such as PRFS thermometry should be particularly aware of errors that can remain despite the use of fat suppression techniques.

Ethical standards

The in vivo experiment was led according to legal ethics regulations (registered project APAFIS #47066-202403251805958).

CRediT authorship contribution statement

Anne Josset: Writing – review & editing, Writing – original draft, Methodology, Investigation, Conceptualization. **Jonathan Vappou:** Writing – review & editing, Supervision, Methodology, Investigation, Conceptualization. **Ounay Ishak:** Writing – review & editing, Methodology, Investigation. **Paolo Cabras:** Writing – review & editing, Supervision, Methodology, Investigation. **Élodie Breton:** Writing – review & editing, Validation, Supervision, Methodology, Investigation, Conceptualization.

Acknowledgments

This work has benefitted from funding of the ANR (Agence Nationale de la Recherche) through the TechnoFUS joint laboratory project (ANR-21-LCV3-0007-01) and MRgHIFU (ANR-21-CE19-0044), and France Life Imaging (ANR-11-INBS-0006). This work was supported by French state funds managed by the ANR within the “Programme d’investissements d’avenir” France 2030 (ANR-10-IAHU-02). This work of the Interdisciplinary Thematic Institute HealthTech, as part of the ITI 2021-2028 program of the University of Strasbourg, CNRS and Inserm, was supported by IdEx Unistra (ANR-10-IDEX-0002) under the framework of the French Investments for the Future Program.

Authors would like to warmfully thank Drs Philippe Garteiser (INSERM Université Paris Cité) and Stanislas Rapacchi (CNRS Aix-Marseille Université) for their scientific input, as well as Drs Khalid Ambarki, Florian Maier, David Grodzki and Nicolas Gross-Weege (Siemens Healthineers) for their input concerning fat suppression and optimized acquisition in our MR scanner.

Appendix A. Supplementary data

Supplementary data to this article can be found online at https://doi.org/10.1016/j.mri.2025.110340.

References

[1] Ishihara Y, Calderon A, Watanabe H, Okamoto K, Suzuki Y, Kuroda K, et al. A precise and fast temperature mapping using water proton chemical shift. Magn Reson Med 1995;34:814–23. https://doi.org/10.1002/mrm.1910340606.
[2] Quesson B, de Zwart JA, Moonen CTW. Magnetic resonance temperature imaging for guidance of thermotherapy. J Magn Reson Imaging 2000;12:525–33. https://doi.org/10.1002/1522-2586(200010)12:4<525::AID-JMRI3>3.0.CO;2-V.
[3] Rieke V, Butts Pauly K. MR thermometry. J Magn Reson Imaging 2008;27:376–90. https://doi.org/10.1002/jmri.21265.
[4] Stollberger R, Ascher PW, Huber D, Radner H, Ebner F. Temperature monitoring of interstitial thermal tissue coagulation using MR phase images. J Magn Reson Imaging 1998;8:188–96. https://doi.org/10.1002/jmri.1880080132.
[5] Rieke V, Butts Pauly K. Echo combination to reduce proton resonance frequency (PRF) thermometry errors from fat. J Magn Reson Imaging 2008;27:673–7. https://doi.org/10.1002/jmri.21238.
[6] Mulkern RV, Panych LP, Hynynen K, Jolesz FA, McDannold NJ. Tissue temperature monitoring with multiple gradient-echo imaging sequences. J Magn Reson Imaging 1998;8:493–502. https://doi.org/10.1002/jmri.1880080234.
[7] Kuroda K, Oshio K, Chung AH, Hynynen K, Jolesz FA. Temperature mapping using the water proton chemical shift: A chemical shift selective phase mapping method. 1997.
[8] Weidensteiner C, Quesson B, Caire-Gana B, Kerioui N, Rullier A, Trillaud H, et al. Real-time MR temperature mapping of rabbit liver in vivo during thermal ablation. Magn Reson Med 2003;50:322–30. https://doi.org/10.1002/mrm.10521.
[9] Lepetit-Coiffé M, Quesson B, Seror O, Dumont E, Le Bail B, Moonen CTW, et al. Real-time monitoring of radiofrequency ablation of rabbit liver by respiratory-gated quantitative temperature MRI. J Magn Reson Imaging 2006;24:152–9. https://doi.org/10.1002/jmri.20605.
[10] Weidensteiner C, Kerioui N, Quesson B, de Senneville BD, Trillaud H, Moonen CTW. Stability of real-time MR temperature mapping in healthy and diseased human liver. J Magn Reson Imaging 2004;19:438–46. https://doi.org/10.1002/jmri.20019.
[11] Seror O, Lepetit-Coiffé M, Le Bail B, Denis De Senneville B, Trillaud H, Moonen C, et al. Real time monitoring of radiofrequency ablation based on MR thermometry and thermal dose in the pig liver in vivo. Eur Radiol 2008;18:408–16. https://doi.org/10.1007/s00330-007-0761-4.
[12] Lepetit-Coiffé M, Laumonier H, Seror O, Quesson B, Sesay M-B, Moonen CTW, et al. Real-time monitoring of radiofrequency ablation of liver tumors using thermal-dose calculation by MR temperature imaging: initial results in nine patients, including follow-up. Eur Radiol 2010;20:193–201. https://doi.org/10.1007/s00330-009-1532-1.
[13] Quesson B, Laurent C, Maclair G, De Senneville BD, Mougenot C, Ries M, et al. Real-time volumetric MRI thermometry of focused ultrasound ablation in vivo: a feasibility study in pig liver and kidney. NMR Biomed 2011;24:145–53. https://doi.org/10.1002/nbm.1563.
[14] Deckers R, Merckel LG, Denis De Senneville B, Schubert G, Köhler M, Knuttel FM, et al. Performance analysis of a dedicated breast MR-HIFU system for tumor ablation in breast cancer patients. Phys Med Biol 2015;60:5527–42. https://doi.org/10.1088/0031-9155/60/14/5527.
[15] Merckel LG, Knuttel FM, Deckers R, van Dalen T, Schubert G, Peters NHGM, et al. First clinical experience with a dedicated MRI-guided high-intensity focused ultrasound system for breast cancer ablation. Eur Radiol 2016;26:4037–46. https://doi.org/10.1007/s00330-016-4222-9.
[16] Adams-Tew SI, Johnson S, Odéen H, Parker DL, Payne A. Validation of a drift-corrected 3D MR temperature imaging sequence for breast MR-guided focused ultrasound treatments. Magn Reson Imaging 2023;96:126–34. https://doi.org/10.1016/j.mri.2022.12.006.
[17] Payne A, Merrill R, Minalga E, Hadley JR, Odeen H, Hofstetter LW, et al. A breast-specific MR guided focused ultrasound platform and treatment protocol: first-in-human technical evaluation. IEEE Trans Biomed Eng 2021;68:893–904. https://doi.org/10.1109/TBME.2020.3016206.
[18] Haase A, Frahm J, Hanicke W, Matthaei D. ^{1}H NMR chemical shift selective (CHESS) imaging. Phys Med Biol 1985;30:341–4. https://doi.org/10.1088/0031-9155/30/4/008.
[19] Kijowski R, Woods MA, Lee KS, Takimi K, Yu H, Shimakawa A, et al. Improved fat suppression using multipeak reconstruction for IDEAL chemical shift fat-water separation: application with fast spin echo imaging. Magn Reson Imaging 2009;29:436–42. https://doi.org/10.1002/jmri.21664.
[20] Hansmann J, Hernando D, Reeder SB. Fat confounds the observed apparent diffusion coefficient in patients with hepatic steatosis. Magn Reson Med 2013;69:545–52. https://doi.org/10.1002/mrm.24535.
[21] Hanniman E, Costa AF, Bowen CV, Abdolell M, Stueck A, McLeod M, et al. Prospective evaluation of virtual MR elastography with diffusion-weighted imaging in subjects with nonalcoholic fatty liver disease. Magn Reson Imaging 2022;56:1448–56. https://doi.org/10.1002/jmri.28154.
[22] Dieckmeyer M, Ruschke S, Eggers H, Kooijman H, Rummeny EJ, Kirschke JS, et al. ADC quantification of the vertebral bone marrow water component: removing the confounding effect of residual fat. Magn Reson Med 2017;78:1432–41. https://doi.org/10.1002/mrm.26550.
[23] Bley TA, Wieben O, François CJ, Brittain JH, Reeder SB. Fat and water magnetic resonance imaging. Magn Reson Imaging 2010;31:4–18. https://doi.org/10.1002/jmri.21895.
[24] Meyer CH, Pauly JM, Macovskiand A, Nishimura DG. Simultaneous spatial and spectral selective excitation. Magn Reson Med 1990;15:287–304. https://doi.org/10.1002/mrm.1910150211.
[25] Zhao Y, Zu Z, Wang Z, Liu Z, Guo B, Yan X, et al. Effectiveness of fat suppression using a water-selective binomial-pulse excitation in chemical exchange saturation transfer (CEST) magnetic resonance imaging. Magnet Resonan Mater Phys Biol Med 2020;33:809–18. https://doi.org/10.1007/s10334-020-00851-7.
[26] Runge VM, Heverhagen JT. Fat suppression: Spectral saturation. In: The physics of clinical MR taught through images. Cham: Springer International Publishing; 2022. p. 98–9. https://doi.org/10.1007/978-3-030-85413-3_46.
[27] Hamilton G, Yokoo T, Bydder M, Cruite I, Schroeder ME, Sirlin CB, et al. In vivo characterization of the liver fat 1H MR spectrum. NMR Biomed 2011;24. https://doi.org/10.1002/nbm.1622.

[28] Yu H, Shimakawa A, McKenzie CA, Brodsky EK, Brittain JH, Reeder SB. Multiecho water-fat separation and simultaneous R2* estimation with multifrequency fat spectrum modeling. Magn Reson Med 2008;60:1122–34. https://doi.org/10.1002/mrm.21737.
[29] Hernando D, Sharma SD, Aliyari Ghasabeh M, Alvis BD, Arora SS, Hamilton G, et al. Multisite, multivendor validation of the accuracy and reproducibility of proton-density fat-fraction quantification at 1.5T and 3T using a fat–water phantom. Magn Reson Med 2017;77:1516–24. https://doi.org/10.1002/mrm.26228.
[30] Bydder M, Girard O, Hamilton G. Mapping the double bonds in triglycerides. Magn Reson Imaging 2011;29:1041–6. https://doi.org/10.1016/j.mri.2011.07.004.
[31] Leporq B, Lambert SA, Ronot M, Vilgrain V, Van Beers BE. Quantification of the triglyceride fatty acid composition with 3.0 T MRI. NMR Biomed 2014;27:1211–21. https://doi.org/10.1002/nbm.3175.
[32] Middleton MS, Hamilton G, Bydder GM, Sirlin CB. How much fat is under the water peak in liver fat MR spectroscopy?. 2009. p. 4331:4331.
[33] Hernando D, Sharma SD, Kramer H, Reeder SB. On the confounding effect of temperature on chemical shift-encoded fat quantification. Magn Reson Med 2014;72:464–70. https://doi.org/10.1002/mrm.24951.
[34] Reeder SB, Wen Z, Yu H, Pineda AR, Gold GE, Markl M, et al. Multicoil Dixon chemical species separation with an iterative least-squares estimation method. Magn Reson Med 2004;51:35–45. https://doi.org/10.1002/mrm.10675.
[35] Daudé P, Roussel T, Troalen T, Viout P, Hernando D, Guye M, et al. Comparative review of algorithms and methods for chemical-shift-encoded quantitative fat-water imaging. Magn Reson Med 2024;91:741–59. https://doi.org/10.1002/mrm.29860.
[36] Dixon WT. Simple proton spectroscopic imaging. Radiology 1984;153:189–94. https://doi.org/10.1148/radiology.153.1.6089263.
[37] Glover GH. Multipoint dixon technique for water and fat proton and susceptibility imaging. J Magn Reson Imaging 1991;1:521–30. https://doi.org/10.1002/jmri.1880010504.
[38] Yu H, McKenzie CA, Shimakawa A, Vu AT, Brau ACS, Beatty PJ, et al. Multiecho reconstruction for simultaneous water-fat decomposition and T2* estimation. J Magn Reson Imaging 2007;26:1153–61. https://doi.org/10.1002/jmri.21090.
[39] Bydder M, Yokoo T, Hamilton G, Middleton MS, Chavez AD, Schwimmer JB, et al. Relaxation effects in the quantification of fat using gradient echo imaging. Magn Reson Imaging 2008;26:347–59. https://doi.org/10.1016/j.mri.2007.08.012.
[40] Wang X, Hernando D, Reeder SB. Sensitivity of chemical shift-encoded fat quantification to calibration of fat MR spectrum. Magn Reson Med 2016;75:845–51. https://doi.org/10.1002/mrm.25681.
[41] Chung AH, Hynynen K, Colucci V, Oshio K, Cline HE, Jolesz FA. Optimization of spoiled gradient-echo phase imaging for in vivo localization of a focused ultrasound beam. Magn Reson Med 1996;36:745–52. https://doi.org/10.1002/mrm.1910360513.
[42] Gorny KR, Favazza CP, Lu A, Felmlee JP, Hangiandreou NJ, Browne JE, et al. Practical implementation of robust MR-thermometry during clinical MR-guided microwave ablations in the liver at 1.5 T. Phys Med 2019;67:91–9. https://doi.org/10.1016/j.ejmp.2019.10.020.
[43] Hynynen K, Pomeroy O, Smith DN, Huber PE, McDannold NJ, Kettenbach J, et al. MR imaging-guided focused ultrasound surgery of fibroadenomas in the breast: a feasibility study. Radiology 2001;219:176–85. https://doi.org/10.1148/radiology.219.1.r01ap02176.
[44] Kuroda K, Oshio K, Mulkern RV, Jolesz FA. Optimization of chemical shift selective suppression of fat. Magn Reson Med 1998;40:505–10. https://doi.org/10.1002/mrm.1910400402.
[45] Sklenár V, Starcuk Z. 1-2-1 pulse train: a new effective method of selective excitation for proton NMR in water. J Magn Reson 1982;50:495–501.
[46] Bush EC, Gifford A, Coolbaugh CL, Towse TF, Damon BM, Welch EB. Fat-water phantoms for magnetic resonance imaging validation: a flexible and scalable protocol. JoVE 2018:57704. https://doi.org/10.3791/57704.
[47] Bing C, Staruch R, Tillander M, Köhler MO, Mougenot C, Ylihautala M, et al. Drift correction for accurate PRF shift MR thermometry during mild hyperthermia treatments with MR-HIFU. Int J Hyperthermia 2016;32:673–87. https://doi.org/10.1080/02656736.2016.1179799.
[48] Odéen H, Parker DL. Magnetic resonance thermometry and its biological applications – physical principles and practical considerations. Prog Nucl Magn Reson Spectrosc 2019;110:34–61. https://doi.org/10.1016/j.pnmrs.2019.01.003.
[49] Pineda AR, Reeder SB, Wen Z, Pelc NJ. Cramér–Rao bounds for three-point decomposition of water and fat. Magn Reson Med 2005;54:625–35. https://doi.org/10.1002/mrm.20623.
[50] Del Grande F, Santini F, Herzka DA, Aro MR, Dean CW, Gold GE, et al. Fat-suppression techniques for 3-T MR imaging of the musculoskeletal system. RadioGraphics 2014;34:217–33. https://doi.org/10.1148/rg.341135130.
[51] Chan TW, Listerud J, Kressel HY. Combined chemical-shift and phase-selective imaging for fat suppression: theory and initial clinical experience. Radiology 1991;181:41–7. https://doi.org/10.1148/radiology.181.1.1887054.
[52] Mao J, Yan H, Brey WW, Bidgood WD, Steinbach JJ, Mancuso A. Fat tissue and fat suppression. Magn Reson Imaging 1993;11:385–93. https://doi.org/10.1016/0730-725X(93)90071-K.
[53] Xu F, Li W, Liu D, Zhu D, Schär M, Myers K, et al. A novel spectrally selective fat saturation pulse design with robustness to B0 and B1 inhomogeneities: a demonstration on 3D T1-weighted breast MRI at 3T. Magn Reson Imaging 2021;75:156–61. https://doi.org/10.1016/j.mri.2020.10.015.
[54] Gianfelice D, Khiat A, Amara M, Belblidia A, Boulanger Y. MR imaging–guided focused US ablation of breast cancer: histopathologic assessment of effectiveness—initial experience. Radiology 2003;227:849–55. https://doi.org/10.1148/radiol.2281012163.
[55] Zippel DB, Papa MZ. The use of MR imaging guided focused ultrasound in breast cancer patients; a preliminary phase one study and review. Breast Cancer 2005;12:32–8. https://doi.org/10.2325/jbcs.12.32.
[56] Furusawa H, Namba K, Thomsen S, Akiyama F, Bendet A, Tanaka C, et al. Magnetic resonance–guided focused ultrasound surgery of breast cancer: reliability and effectiveness. J Am Coll Surg 2006;203:54–63. https://doi.org/10.1016/j.jamcollsurg.2006.04.002.
[57] Todd N, Diakite M, Payne A, Parker DL. In vivo evaluation of multi-echo hybrid PRF/T1 approach for temperature monitoring during breast MR-guided focused ultrasound surgery treatments. Magn Reson Med 2014;72:793–9. https://doi.org/10.1002/mrm.24976.
[58] Zhang L, Armstrong T, Li X, Wu HH. A variable flip angle golden-angle-ordered 3D stack-of-radial MRI technique for simultaneous proton resonant frequency shift and T_1 -based thermometry. Magn Reson Med 2019;82:2062–76. https://doi.org/10.1002/mrm.27883.
[59] Lena B, Bartels LW, Ferrer CJ, Moonen CTW, Viergever MA, Bos C. Interleaved water and fat MR thermometry for monitoring high intensity focused ultrasound ablation of bone lesions. Magn Reson Med 2021;86:2647–55. https://doi.org/10.1002/mrm.28877.
[60] Hey S, de Smet M, Stehning C, Grüll H, Keupp J, Moonen CTW, et al. Simultaneous T1 measurements and proton resonance frequency shift based thermometry using variable flip angles. Magn Reson Med 2012;67:457–63. https://doi.org/10.1002/mrm.22987.
[61] Todd N, Diakite M, Payne A, Parker DL. Hybrid proton resonance frequency/T1 technique for simultaneous temperature monitoring in adipose and aqueous tissues. Magn Reson Med 2013;69:62–70. https://doi.org/10.1002/mrm.24228.
[62] Baron P, Ries M, Deckers R, de Greef M, Tanttu J, Köhler M, et al. In vivo T2-based MR thermometry in adipose tissue layers for high-intensity focused ultrasound near-field monitoring. Magn Reson Med 2014;72:1057–64. https://doi.org/10.1002/mrm.25025.
[63] Ozhinsky E, Han M, Bucknor M, Krug R, Rieke V. T2-based temperature monitoring in bone marrow for MR-guided focused ultrasound. J Ther Ultrasound 2016;4:26. https://doi.org/10.1186/s40349-016-0073-8.
[64] Kuroda K, Iwabuchi T, Obara M, Honda M, Saito K, Imai Y. Temperature dependence of relaxation times in proton components of fatty acids. MRMS 2011;10:177–83. https://doi.org/10.2463/mrms.10.177.